Current Topics/Perspectives

Applications of Phospholipid Bilayer Nanodiscs in the Study of Membranes and Membrane Proteins

Abhinav Nath, William M. Atkins, and Stephen G. Sligar

Biochemistry, **2007**, 46 (8), 2059-2069 • DOI: 10.1021/bi602371n

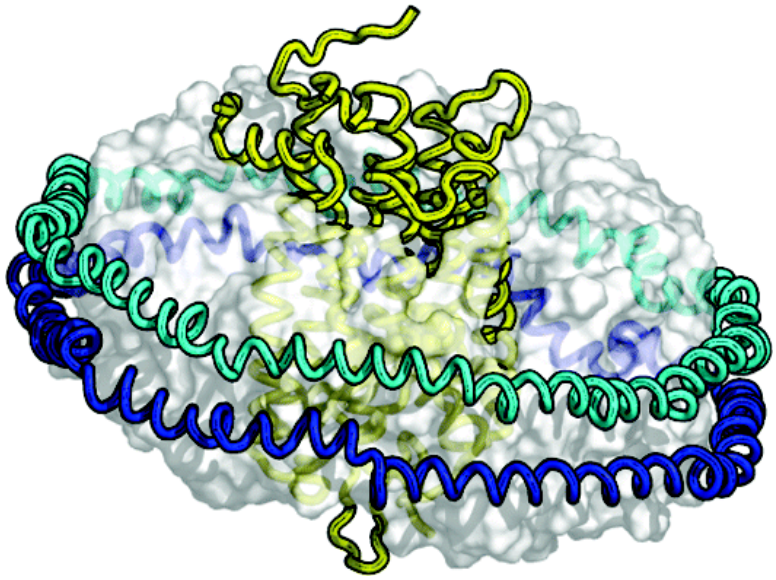

BIOCHEMISTRY

 Volume 46, Number 8 February 27, 2007

Current Topics

Applications of Phospholipid Bilayer Nanodiscs in the Study of Membranes and Membrane Proteins†

Abhinav Nath,‡ William M. Atkins,*,‡ and Stephen G. Sligar*,§

Department of Medicinal Chemistry, University of Washington, Seattle, Washington 98195, and Department of Biochemistry, University of Illinois, Urbana, Illinois 61801

Received November 15, 2006; Revised Manuscript Received December 28, 2006

ABSTRACT: Phospholipid bilayer Nanodiscs are novel model membranes derived from high-density lipoprotein particles and have proven to be useful in studies of membrane proteins. Membrane protein enzymology has been hampered by the inherent insolubility of membrane proteins in aqueous environments and has necessitated the use of model membranes such as liposomes and detergent-stabilized micelles. Current model membranes display a polydisperse particle size distribution and can suffer from problems of inconsistency and instability. It is also unclear how well they mimic biological lipid bilayers. In contrast, Nanodiscs, the particle size of which is constrained by a coat of scaffold proteins, are relatively monodisperse, stable model membranes with a "nativelike" lipid bilayer. Nanodiscs have already been used to study a variety of membrane proteins, including cytochrome P450s, seven-transmembrane proteins, and bacterial chemoreceptors. These proteins are simultaneously monomerized, solubilized, and incorporated into the well-defined membrane environment provided by Nanodiscs. Nanodiscs may also provide useful insights into the thermodynamics and biophysics of biological membranes and binding of small molecules to membranes.

Membrane proteins are involved in numerous vital biological processes, including transport, signal transduction, and a variety of metabolic pathways. Integral membrane proteins may account for up to 30% of the human proteome (*1*) and make up approximately half of all currently marketed therapeutic targets (*2*, *3*). Unfortunately, membrane proteins are inherently recalcitrant to study using the toolkit available to modern enzymologists. The heterologous expression of recombinant membrane proteins has proven to be difficult and often results in low yields or fails to recapture the post-translational modifications present in the native protein (*4*). Even if sufficient quantities of the protein of interest can be isolated for study, common biophysical techniques such as X-ray crystallography, NMR,[1] fluorescence, and circular dichroism or absorbance spectroscopy work best with soluble proteins. Membrane proteins are inherently insoluble or prone to aggregation and oligomerization in solution. To circumvent these limitations, biochemists have relied on a wide variety of model membranes and detergent systems (see ref *5* for an excellent review), but in some cases, it is unclear how well these systems mimic the native membrane protein

† This work was supported by National Institutes of Health Grants GM-32165, GM-62284 and GM-33775.

* To whom correspondence should be addressed. W.M.A.: Department of Medicinal Chemistry, Box 357610, University of Washington, Seattle, WA 91895-7610; phone, (206) 685-0379; fax, (206) 685-3252; e-mail, winky@u.washington.edu. S.G.S.: Department of Biochemistry, University of Illinois, 505 S. Goodwin Ave., Urbana, IL 61801; e-mail, s-sligar@uiuc.edu.

‡ University of Washington.

§ University of Illinois.

10.1021/bi602371n CCC: $37.00
Published on Web 01/31/2007

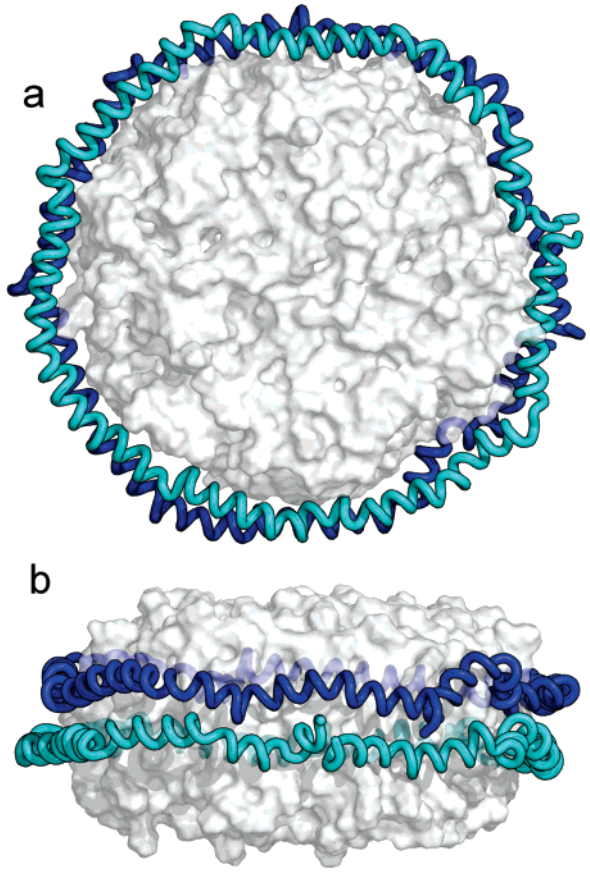

FIGURE 1: Model of Nanodisc structure viewed (a) perpendicular to the bilayer and (b) in the plane of the bilayer, based on the molecular belt model of discoidal HDL (*47*). Two monomers of the membrane scaffold protein (blue and cyan) form an amphipathic helical belt around a segment of phospholipid bilayer (in white) ~10 nm in diameter. The model is courtesy of S. C. Harvey.

system; they may adversely affect a membrane protein's structure and dynamics to poorly reflect in vivo behavior. A method of maintaining membrane proteins monomerically in a nativelike bilayer, while simultaneously in solution, would greatly extend the accuracy, power, and facility of membrane protein enzymology.

In this work, we describe phospholipid bilayer Nanodiscs (*6*−*8*), a new class of model membranes with several attractive properties that may help satisfy this inadequacy in the study of membrane proteins. Nanodiscs consist of a segment of phospholipid bilayer surrounded by a protein coat of defined and controllable size (see the structural model in Figure 1). They present distinct advantages over currently used model membranes in terms of particle size monodispersity and consistency: the presence of the protein belt constrains the dimensions of the bilayer and ensures that Nanodisc particle size distributions tend to be more monodisperse (within a single preparation) and consistent (between preparations) than current model membranes such as liposomes and detergent-stabilized micelles. The protein coat also makes Nanodiscs relatively stable over time. Additionally, there is evidence that Nanodiscs better reflect the complex phase transition behavior of biological membranes than conventional model membranes (*9*, *10*).

As model membranes, Nanodiscs have the potential to greatly enhance our understanding of membrane proteins. A membrane protein incorporated into Nanodiscs is simultaneously solubilized, monomerized, and incorporated into a well-defined phospholipid bilayer. Nanodiscs therefore provide a way to study membrane proteins in a close-to-native membrane environment using a wide variety of solution- and surface-based techniques. A variety of membrane proteins (Figure 5) have been incorporated into Nanodiscs, including cytochrome P450s (CYPs) (*11*−*16*), NADPH-cytochrome P450 reductase (CPR) (*17*, *18*), bacteriorhodopsin (*19*, *20*), G protein-coupled receptors (GPCRs) (*21*), and bacterial chemoreceptors (*22*). Nanodiscs can thus be used to study a wide variety of interesting and biologically significant membrane proteins.

The well-defined nature of the Nanodisc bilayer also makes them attractive systems for studying binding of small molecules to membranes. The energetics of binding of small molecules to liposomes, for instance, are known to be affected by vesicle size (*23*). Using a monodisperse model membrane of known size enables a more detailed and accurate understanding of how a given small molecule binds to membranes. The stable and soluble nature of Nanodiscs allows the use of a variety of steady-state and kinetic experimental techniques (including stopped-flow spectroscopy). A rigorous understanding of binding of ligand to Nanodiscs is a necessary prerequisite for any studies of binding of ligand to incorporated proteins.

Structurally, Nanodiscs strongly resemble nascent discoidal high-density lipoprotein (HDL) particles; the scaffold proteins that make up their protein coats are derived from apolipoprotein A-I (apoA-I). This provides a rich pool of information about the structure and dynamics of Nanodiscs, since the properties of HDL particles have been extensively studied. We will briefly review structural models of HDL particles, experimental information regarding Nanodiscs themselves, molecular dynamics simulations of both HDL particles and Nanodiscs, and finally Nanodiscs' experimental utility as model membranes, both in terms of understanding small-molecule binding and in terms of enhancing our knowledge of membrane proteins.

Structure and Function of ApoA-I and HDL Particles

The primary role of HDL particles and apoA-I in vivo is in reverse cholesterol transport (RCT) (*24*, *25*), a process by which accumulated cholesterol is transported from tissues all over the body to the liver for excretion. Two apoA-I monomers bind to serum phospholipids to form nascent discoidal HDL (ndHDL) particles, which interact with ATP-binding cassette transporter A1 (ABCA1); cholesterol is then

[1] Abbreviations: CYP, cytochrome P450; CPR, NADPH-cytochrome P450 reductase; GPCR, G protein-coupled receptor; HDL, high-density lipoprotein; apo, apolipoprotein; RCT, reverse cholesterol transport; ndHDL, nascent discoidal HDL; ABCA1, ATP-binding cassette transporter A1; LCAT, lecithin:cholesterol acyltransferase; EPR, electron paramagnetic resonance; FRET, fluorescence resonance energy transfer; NMR, nuclear magnetic resonance; MSP, membrane scaffold protein; SEC, size-exclusion chromatography; AFM, atomic force microscopy; SAXS, small-angle X-ray scattering; DPPC, dipalmitoylphosphatidylcholine; DMPC, dimyristoylphosphatidylcholine; POPC, palmitoyloleoylphosphatidylcholine; MLV, multilamellar vesicle; LUV, large unilamellar vesicle; SUV, small unilamellar vesicle; PEG, polyethylene glycol; DSC, differential scanning calorimetry; 7-TM, seven-transmembrane; bR, bacteriorhodopsin; CD, circular dichroism; β_2AR, β_2-adrenergic receptor; HEK, human embryonic kidney; *t*-CA, *tert*-cinnamic acid.

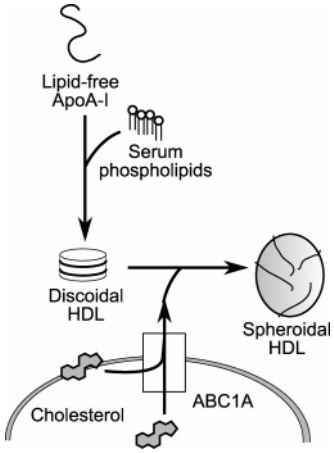

FIGURE 2: Physiological role of apoA-I and discoidal HDL in reverse cholesterol transport. Lipid-free apoA-I, which dynamically samples an ensemble of conformations, binds to serum phospholipids to form nascent discoidal HDL particles. Cholesterol effluxed from cells by passive diffusion, ABC1A and other transporters, is taken up by discoidal HDL and esterified by LCAT. This causes the conversion of discoidal HDL particles to spheroidal particles, which transport cholesteryl esters to the liver.

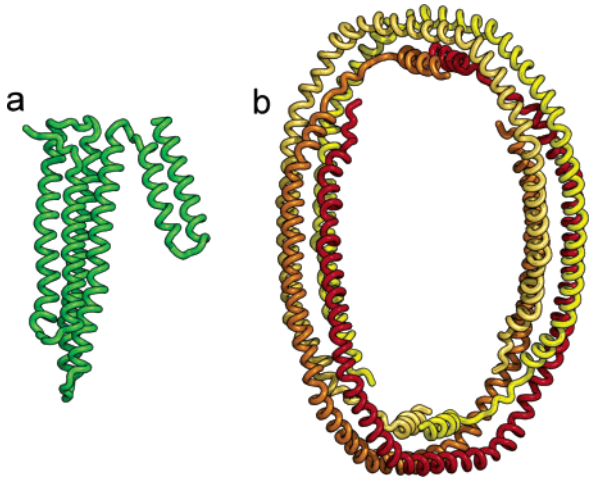

FIGURE 3: Crystal structures of apoA-I. (a) The full-length protein (*35*), PDB entry 2A01, displays a compact α-helical structure with an N-terminal four-helix bundle and two C-terminal helices. Lipid-free apoA-I displays a lower α-helical content in solution (*32*, *33*) than that observed in this crystal structure, suggesting that the protein dynamically samples multiple conformations. (b) The N-terminal truncation apoA-I(Δ[1−43]) has four monomers (in four different colors) in the asymmetric unit, arranged in a cylindrical belt of amphipathic helices. In solution, this truncated protein resembles discoidal HDL in terms of α-helical content and proteolytic cleavage patterns (*34*, *37*, *38*), suggesting it is a good qualitative model for discoidal HDL particles.

transported from the cell membrane into the ndHDL particles in an ATP-dependent process. Cholesterol is incorporated in the HDL particles via esterification by lecithin:cholesterol acyltransferase (LCAT). As they absorb increasing quantities of cholesteryl esters, ndHDL particles are transformed into mature spheroidal HDL particles, which can incorporate up to four apoA-I molecules, as well as apoA-II (see the overview in Figure 2).

ApoA-I is a 243-residue protein, with a largely α-helical N-terminal globular domain ∼43 residues in length; the rest of the protein displays considerable conformational heterogeneity in solution (*26*). HDL particles can be reconstituted in vitro by mixing apoA-I with a detergent-solubilized phospholipid; discoidal HDL particles are formed at lipid:apoA-I ratios in the range of 100:1, whereas spheroidal particles form at higher lipid:apoA-I ratios. Particle size can vary from 7.8 to ∼13 nm, depending of the precise ratio of apoA-I to phospholipid used in the reconstitution mixture (*27*−*29*). A similar range of particle sizes is found in discoidal HDL isolated from human plasma (*30*).

Two naturally occurring apoA-I mutants have interesting properties: apoA-I_{Milano} (R173C) and apoA-I_{Paris} (R151C) (*31*). Both result in decreased levels of HDL in vivo but appear to protect heterozygotic individuals from atherosclerosis. The protective effect of these mutations may be due to some combination of more stable HDL particles and a decreased efficiency of interaction with LCAT. Both mutants are capable of forming reconstituted HDL particles, albeit as disulfide-linked homodimers.

Published values for the α-helical content of lipid-free apoA-I measured by circular dichroism vary from 50 (*32*) to 68% (*33*), depending on the experimental conditions; discoidal HDL particles show an increase in α-helical content to ∼80% (*34*). Two crystal structures of apoA-I exist, one (PDB entry 2A01, Figure 3a) of the full-length protein at 2.4 Å resolution (*35*) and the other (PDB entry 1AV1, Figure 3b) of the N-terminal truncation apoA-I(Δ[1−43]) at 4.0 Å resolution (*36*). Both crystal structures exhibit extensive amphipathic α-helix formation: ∼80% for the full-length structure and ∼85% for the N-terminal truncation. However, the overall folds are quite dissimilar. The full-length crystal structure displays an extensive N-terminal four-helix bundle and two shorter C-terminal helices, with most contact between hydrophobic residues occurring within the same monomer; in contrast, the N-terminal truncation crystal structure shows four apoA-I monomers in a cylindrical belt composed of 10 amphipathic α-helices, with substantial intermonomer hydrophobic contact. Interestingly, in solution, apoA-I(Δ[1−43]) more closely resembles lipid-bound apoA-I than the lipid-free form in terms of α-helical content (*33*, *34*, *37*) and proteolytic cleavage patterns (*37*, *38*). Taken together, these data suggest that lipid-free apoA-I dynamically samples multiple conformations in solution (some of which may be represented by the full-length crystal structure, while others display much less helical structure) but that the conformation of lipid-bound apoA-I (i.e., discoidal HDL particles) qualitatively resembles the truncated crystal structure.

Lipoprotein particle structure has been the subject of study for 30 years (*39*−*43*). A number of structural models of discoidal HDL have been proposed (*26*, *41*, *43*), varying in the conformation adopted by apoA-I. In the "picket fence" model (*44*, *45*) (Figure 4a), the two monomers of apoA-I are arranged on opposite sides of the phospholipid bilayer, with short antiparallel helices arranged perpendicular to the plane of the bilayer. In the "molecular belt" model (*31*, *46*, *47*) (Figure 4b), two monomers of apoA-I are arranged head to tail with their helices parallel to the plane of the membrane (and their hydrophobic residues in contact with the lipid tail groups), extended all the way around the bilayer. A variant of the molecular belt model is the "hairpin" (*48*) (Figure 4c), where the two apoA-I monomers are on opposite sides of the bilayer. Lately, a consensus has emerged in the literature, with results from polarized internal reflection

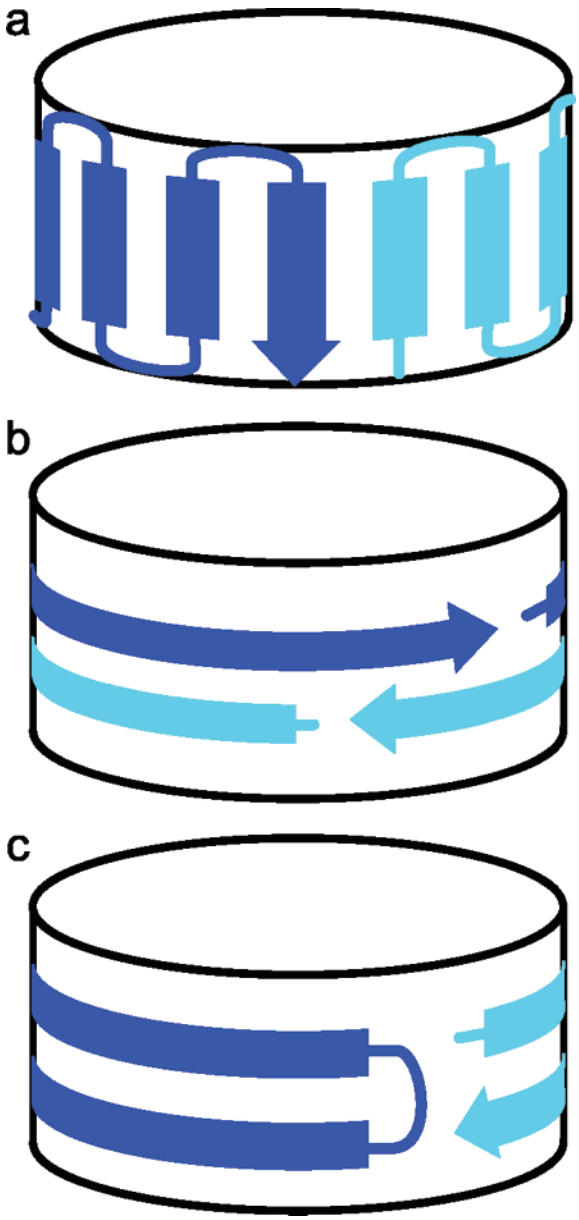

FIGURE 4: Proposed structural models of discoidal HDL. (a) The picket fence model (*44*, *45*) features two apoA-I monomers on opposite sides of the particle, with short antiparallel helices arranged perpendicular to the plane of the bilayer. (b) The molecular belt model (*31*, *46*, *47*) has two monomers extended head to tail around the bilayer. See Figure 1 for a more detailed view of this model. The molecular belt model is most strongly supported by experimental evidence (*46*, *49*−*56*, *93*). (c) The hairpin model (*48*) still has the monomers on opposite sides, but with amphipathic helices parallel to the plane of the membrane.

infrared spectroscopy (*46*), cross-linking/mass spectrometry (*49*−*52*), mutagenesis (*53*), EPR (*54*), fluorescence spectroscopy (*55*), FRET (*54*, *56*), and solid-state NMR (*57*) strongly supporting the molecular belt model.

Detailed molecular models of discoidal HDL particles (*31*, *47*, *58*) (Figure 1) have been published. These have been determined by arranging apoA-I in a toroid amphipathic helix to orient the hydrophobic face inward. (This structure is an idealized amphipathic 11/3-helix, with an average pitch of 3.67 residues/turn, as compared to the pitch of 3.6 residues/turn for the canonical α-helix.) Two apoA-I monomers were arranged head to tail, and their register was adjusted to maximize the number of intermonomer salt bridges; a segment of phospholipid bilayer from a molecular dynamics simulation (*59*) was inserted into the resulting ring. These HDL particle models provide a good schematic of the overall size and topology of Nanodiscs.

Nanodisc Structure

Nanodiscs consist of a membrane scaffold protein (MSP), a derivative of apoA-I, surrounding a bilayer of phospholipid molecules. Initial MSP constructs (*6*) were MSP1 [the apoA-I(Δ[1−43]) sequence] and MSP2 [two copies of apoA-I(Δ-[1−43]) attached head to tail with a short linker]. All subsequent MSP constructs (*7*) also lack the N-terminal globular domain of apoA-I, which is not thought to interact directly with the lipid bilayer at the lipid ratios used in Nanodisc assembly.

Nanodiscs are assembled by adding MSP to a detergent-stabilized phospholipid in a suitable molar ratio and then removing the detergent from the mixed micelles. In practice, the detergent is cholic acid (used in a 2-fold molar excess to the phospholipid), and its removal is achieved either by dialysis into buffer or by using hydrophobic adsorbents such as Bio-Beads SM-2 (Bio-Rad, Hercules, CA). This is essentially the same procedure that was used to create reconstituted discoidal HDL particles.

Initially, Nanodiscs were assembled using two molecules of MSP1, or one molecule of MSP2, with dipalmitoylphosphatidylcholine (DPPC) and palmitoyloleoylphosphatidylcholine (POPC) (*6*). POPC has a larger surface area in a bilayer than DPPC, so the molar ratios of lipids used in reconstitution varied: 150 POPC molecules per disc (i.e., a 1:75 molar ratio with MSP1 and a 1:150 molar ratio with MSP2) or 200 DPPC molecules per disc (i.e., 1:100 MSP1:DPPC and 1:200 MSP2:DPPC molar ratios). Experiments with tritiated lipids indicated that ∼160 DPPC or ∼130 POPC molecules were actually incorporated into Nanodiscs. Size-exclusion chromatography (SEC) and atomic force microscopy (AFM) showed that Nanodisc diameter was not significantly affected by which scaffold protein or lipid was used.

Nanodisc size can be precisely controlled by changing the sequence of the MSP construct. Denisov et al. (*7*) prepared a library of MSP constructs of varying length, used them to create Nanodiscs of different sizes, and measured their dimensions by fitting small-angle X-ray scattering (SAXS) data to cylindrical core−shell models. Starting from the MSP1 sequence (which gives Nanodiscs 9.8 nm in diameter), the authors inserted one (MSP1E1), two (E2), and three (E3) 22-mer amphipathic helices to give Nanodiscs 10.6, 11.9, and 12.9 nm in diameter, respectively. In contrast, 11- and 22-residue deletions (MSP1D1 and -D2, respectively) at the N-terminus had little effect on Nanodisc diameter, suggesting that these N-terminal residues do not interact with the bilayer at the lipid ratios used and are not necessary for Nanodisc formation. Size-exclusion chromatography confirmed the particle sizes obtained from SAXS and indicated that the Nanodisc variants were each relatively homogeneous. SAXS also showed that the thickness of the lipid bilayer was ∼5.6 nm for DPPC Nanodiscs and 4.6 nm for POPC Nanodiscs under the experimental conditions (293 K). Linear dichroism experiments (*19*) have also verified that the orientation of the bilayer in Nanodiscs on a surface is similar to that observed for glass-supported lipid bilayers.

Nanodisc structure has also been investigated using solid-state NMR techniques (*57*). MSP1 was uniformly labeled with ^{13}C and ^{15}N and used to prepare dimyristoylphosphatidylcholine (DMPC) Nanodiscs. These were then precipitated in 40% PEG 3350 and studied using magic-angle spinning solid-state NMR. Chemical shifts of unambiguously identified amino acid residues (Ala, Val, Gly, Pro, Ser, Thr, and Glu) indicated that these residues were predominantly in α-helical conformations. Additionally, analysis indicated that proline chemical shifts were more consistent with the double-belt model than the picket fence model.

Computational Studies

Discoidal HDL particles and Nanodiscs have been the targets of several molecular dynamics studies (*45*, *60*−*63*). These simulations provide some support for the structural models discussed earlier and provide interesting information about the dynamics of these particles that may explain how their structure changes in response to different amounts of free phospholipids in the environment. However, due to computational limitations, it has not been possible to use molecular dynamics to study the necessary timescales (in the microsecond to millisecond range) with the necessary atomic resolution to arrive at firm conclusions.

In general, the starting models are constructed by taking lipid molecules from simulations of bilayers (*59*, *64*, *65*). ApoA-I monomers are then arranged around the resulting segment of bilayer in accordance with the model being investigated, and steric clashes with lipids are eliminated. The system is then solvated and energy-minimized, and a molecular dynamics trajectory of the desired length is run. In early work, Phillips et al. (*45*) used a combination of simulated annealing and molecular dynamics to compare head-to-head and head-to-tail variants of the HDL picket fence model. Given the short time course of the combined simulations (<100 ps), the final models did not differ significantly from the initial models, and neither variant was markedly more stable than the other. Subsequently, Klon et al. (*60*) performed 1 ns molecular dynamics simulations on double-belt HDL models with wild-type apoA-I (*47*) and apoA-I_{Milano} (*31*). Klon et al. also created a "rotamer" model using wild-type apoA-I, where the register of the two apoA-I monomers was changed by four residues, to abolish the intermonomer salt bridges in the original model. The authors observed that all three models were stable and that the altered rotamer model recovered many intermonomer salt bridges. This suggests that the register of apoA-I in HDL particles is dynamic on a fairly rapid (∼10 ns) time scale. It was also observed that apoA-I proline residues tended to align with each other, suggesting that they also influence the apoA-I register. Catte et al. (*63*) simulated HDL particles with lipid:protein ratios lower than those of the discoidal particles, in an effort to study the process of discoidal HDL formation. Lipid-poor HDL particles rapidly converged on structures similar to the lipid-free crystal structure of apoA-I(Δ[1−43]) (*36*), suggesting that this structure is indeed a good model for intermediates in formation of discoidal HDL. Most recently, Shih et al. (*61*) presented longer (≥4.5 ns) simulations of Nanodiscs made with MSP1, MSP1D1 (Δ[1−11]), and MSP1D2 (Δ[1−22]) and found that MSP1 Nanodiscs were less stable and tended to "buckle" or deform out of the plane of the disc, presumably due to underpacking with phospholipids. Nanodiscs made using the truncated MSP constructs stably retained their discoidal structure. This supports the observation based on SAXS data (*7*) that the 11 or 22 N-terminal residues of MSP1 do not contact the bilayer. A subsequent work (*62*) used coarse-grained molecular dynamics to study Nanodisc formation on the microsecond time scale. Nanodisc self-assembly was simulated starting from an intact lipid bilayer, randomly dispersed lipid molecules, and a lipid micelle. The resultant particles (after 1 or 1.5 μs) resembled Nanodiscs in terms of overall particle size but in some cases were qualitatively closer to the picket fence model than the double-belt model. It is unclear whether these structures resemble actual intermediates in Nanodisc self-assembly or are artifacts of the simulation process.

Utility of Nanodiscs as Model Membranes

Before we describe the properties of Nanodiscs that make them attractive and powerful model membranes, it is worth considering some of the model membranes currently in use (*5*). Liposomes (*66*), first prepared by Bangham (*67*, *68*), are vesicles of amphiphilic lipid bilayers. Liposomes may occur as multilamellar vesicles (MLVs), with several concentric lipid bilayers, or as large (LUVs) or small unilamellar vesicles (SUVs). Numerous methods of liposome preparation have been described (*69*); the best known, and least demanding in terms of specialized equipment, is the so-called Bangham method (hydration of dry lipid films). Here, the lipid of interest is dissolved in a volatile organic solvent and then dried under a stream of inert gas. Liposomes are prepared simply by shaking or vortexing the resulting thin lipid films with an aqueous buffer. This results in a population of MLVs that are heterogeneous in terms of size.

MLVs can be converted to unilamellar vesicles by a variety of processes such as sonication, homogenization, freeze−thaw cycles, reverse phase evaporation, and extrusion through a filter of a known size. All these procedures result in a heterogeneous population of unilamellar vesicles whose final size distribution is sensitive to slight changes in experimental conditions and which generally have some residual MLV content. These experimental considerations cause unavoidable variability between liposome preparations in different laboratories, between different preparations in the same laboratory, and between individual liposomes in the same preparation. Although procedures for preparing more homogeneous, stable, and reproducible liposome populations exist (*70*, *71*), these require unusual equipment and exotic solvents and are not widely used.

The other class of commonly used model membrane is the detergent-stabilized micelle (*72*). Mixed micelles self-assemble when a lipid is mixed with a detergent (when the detergent is above its critical micellar concentration). Micelles are roughly spherical particles with the polar moieties of the detergent and phospholipids forming the outer layer, and hydrophobic moieties forming the core. As model membranes, micelles have the inherent and considerable disadvantage of not being lipid bilayers. It is therefore unclear how well micelles mimic biological membranes, especially with regard to their effect on incorporated membrane proteins. As the ratio of lipid to detergent increases, spherical micelles are converted to vesicles (i.e., liposomes) via a set

of poorly defined intermediates (*73*). Depending on the combination of detergent and lipid, and their relative concentrations, the micelle-to-vesicle intermediates may be some mixture of detergent-bound bilayer disks, flexible threadlike micelles, and other undetermined forms (*74*). While micelle preparations are more reproducible than liposomes, they suffer from the same problems of polydispersity and instability.

Finally, polyethylene glycol (PEG)-stabilized lipid bilayer disks (*75*−*78*) are a promising new class of model membranes. These bilayer disks are discoidal micelles prepared by mixing PEGylated lipids with phospholipids and cholesterol in specific molar ratios. Like liposomes, they possess well-defined lipid bilayers; like micelles, their preparations are relatively reproducible. The average particle size can be tuned by changing the ratios and concentrations of the various constituents. Unfortunately, PEG-stabilized bilayer disks also appear to exhibit a polydisperse particle size distribution.

This then gives us a sense of the ways in which phospholipid bilayer Nanodiscs improve upon other model membranes. (1) Nanodiscs present a biologically relevant, well-defined phospholipid bilayer. (2) Nanodisc particle size distributions are effectively monodisperse and reproducible. (3) The particle size can be tuned with a high degree of precision by altering the MSP sequence. (4) Nanodiscs are relatively robust and stable in solution over a wide range of temperatures. We will now discuss specific examples of Nanodiscs being used as model membranes.

Nanodiscs have provided valuable information about membrane biophysics. Studies of phase transitions in DMPC and DPPC Nanodiscs by differential scanning calorimetry (DSC) and laurdan fluorescence showed that lipid phase transitions in Nanodiscs are broadened and occur at temperatures slightly higher than those of the same lipids in liposomes (*9*). This indicates that fewer lipids make up the cooperative unit for phase transitions in Nanodiscs than in liposomes. The cooperative unit is intrinsically limited to the number of lipids in the Nanodisc; however, it is further limited by the presence of "boundary lipids" lipid molecules that are in direct contact with the protein coat and, therefore, do not participate in phase transitions. Subsequent experiments with DSC, laurdan fluorescence, and SAXS showed that phase transitions are narrower for larger MSP1E3 Nanodiscs than for smaller MSP1 Nanodiscs and that the boundary layer is approximately two lipid molecules thick (*10*). Proteoliposomes exhibit similar behavior, with phase transitions becoming broader as the protein content increases (*79*), and biological membranes contain a substantial amount of protein. This suggests that Nanodiscs better recapture the phase transition behavior of biological membranes than liposomes.

Membrane Proteins Studied using Nanodiscs

The study of membrane proteins has been hampered by the lack of a suitable well-defined, soluble model membrane. In the absence of a model membrane, even relatively soluble membrane proteins will tend to oligomerize and aggregate and thereby complicate experimental results. On the other hand, if liposomes or micelles are used to stabilize proteins, the situation is complicated by these systems' inherent polydispersity, inconsistency, and instability. It has therefore been difficult to use solution-based techniques to obtain rigorous, unambiguous information about membrane protein structure and function. Nanodiscs may provide a valuable adjunct to and extension of conventional model membrane technology.

Several integral membrane proteins (Figure 5) have been incorporated into Nanodiscs, including cytochrome P450s (CYPs) and seven-transmembrane segment (7-TM) proteins. The 7-TM protein bacteriorhodopsin (bR) was incorporated monomerically into Nanodiscs (*19*) by solubilizing bR-containing purple membranes with Triton X-100 and mixing them with MSP1, DMPC, and cholate. Detergent was then removed from the resulting mixed micelles using Bio-Beads SM-2, and Nanodiscs self-assembled with incorporated bR. Molar ratios of the components were adjusted to give a 5-fold excess of Nanodiscs to bR monomers in the final mixture, ensuring that bR was incorporated monomerically. The structural homogeneity and stability of bR-Nanodiscs were verified using SEC, AFM, and electron microscopy, and circular dichroism (CD) measurements verified that incorporated bR was monomeric. bR in Nanodiscs appeared to retain its activity: it bound all-*trans*-retinal with an affinity close to that observed for bR in purple membranes and also displayed similar light−dark difference absorbance spectra. Molecular dynamics simulations of bacteriorhodopsin incorporated into Nanodiscs (*61*) showed that the complex was stable over 4.5 ns. Subsequently, trimeric bR was incorporated into Nanodiscs made with MSP1E2 and MSP1E3, which have larger bilayer areas (*20*). The ratios of Nanodisc components (MSP and DMPC) were chosen to yield equimolar amounts of bR trimers and Nanodiscs in the final mixture. The amount of lipid used in the reconstitution had to be reduced, to account for the area of the Nanodisc bilayer occupied by a bR trimer. CD spectra of bR-Nanodiscs showed a bilobed pattern characteristic of bR trimers, and SAXS measurements showed increased density close to the center of bR-Nanodiscs, consistent with incorporation of bR into the bilayer.

β_2-Adrenergic receptor (β_2AR), a GPCR, and another 7-TM protein have also been incorporated into Nanodiscs (*21*). β_2AR was expressed in HEK293 cells, solubilized using dodecyl β-D-maltoside, and mixed with MSP1 and cholate-solubilized POPC in molar ratios to yield a 75-fold excess of Nanodiscs upon detergent removal. A C-terminal FLAG affinity tag on β_2AR was used to separate β_2AR-Nanodiscs from free Nanodiscs. This ensured that all incorporated β_2-AR was monomeric. The size and stoichiometry of the β_2-AR−Nanodisc complex were verified by SEC and SDS−PAGE, respectively. β_2AR-Nanodiscs retained the ability to bind β_2AR agonists and antagonists and could induce the uptake of GTP analogues by the soluble G protein $G_{s\alpha}$. This showed that β_2AR-Nanodiscs are fully functional, in contrast to detergent-stabilized β_2AR (which does not display G protein coupling). Nanodiscs are thus a suitable model membrane system for solubilizing and studying functional 7-TM proteins.

Nanodiscs have found many applications in the study of microsomal CYPs, which are integral membrane proteins with an N-terminal helical membrane anchor. In early experiments, reconstituted HDL particles (using full-length apoA-I instead of MSP) were used to study the structure of CYP2B4 (*11*) and CPR (*17*, *18*) in a lipid bilayer. The target

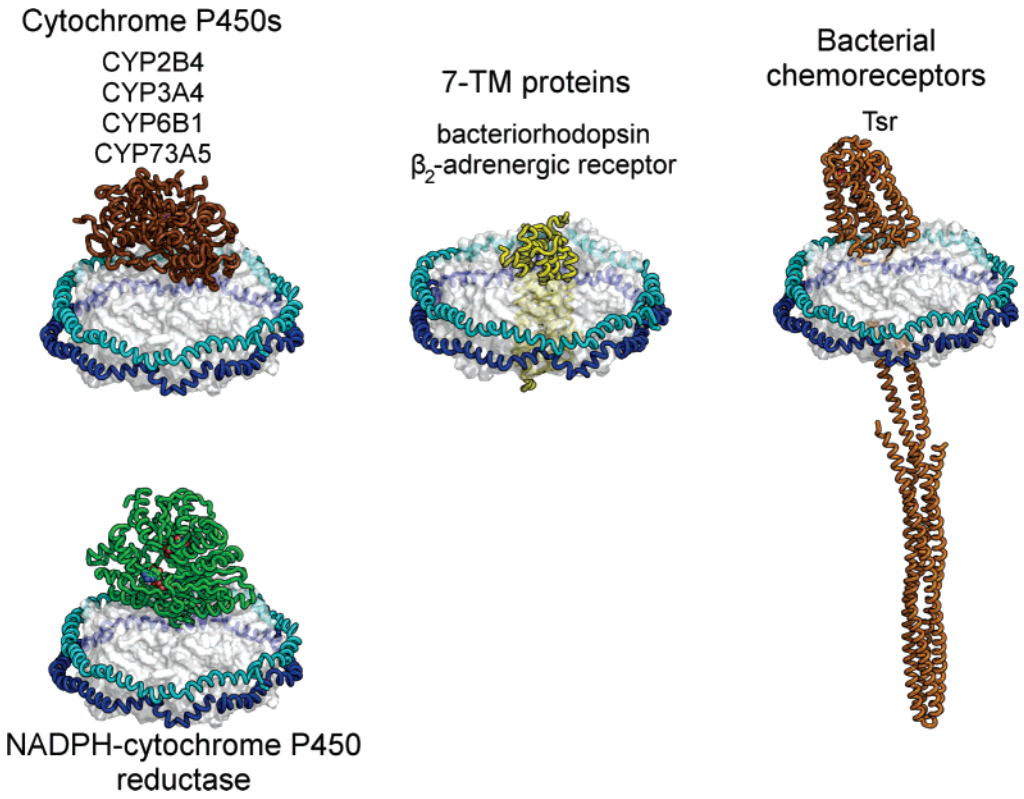

FIGURE 5: Membrane proteins that have been incorporated into Nanodiscs include CYPs, CPR, 7-TM proteins, and bacterial chemoreceptors. Models were constructed in Pymol (*94*) by manually docking crystal structures of CYP3A4 (*95*), CPR (*81*), rhodopsin (*96*), or the cytoplasmic domain of Tsr (*91*) and the periplasmic domain of Tar (*97*) with a discoidal HDL model.

proteins were incubated with apoA-I and detergent-stabilized DPPC to yield an equimolar mixture of target and Nanodisc, and detergent was removed by dialysis. Nanodiscs with incorporated protein were then analyzed by contact-mode and tapping-mode AFM, in an effort to determine the orientation and depth of these membrane proteins in lipid bilayers. The average height of single molecules of CYP2B4 and CPR above the lipid bilayer was found to be ~3.5 (*11*) and ~5.5 nm (*18*), respectively. This is consistent with crystal structures of CYP2B4 (*80*) and CPR (*81*), but the uncertainties in these values prevented an unambiguous determination of the orientation relative to the membrane.

Interestingly, Nanodiscs have been used to directly solubilize recombinant CYPs from an insect cell expression system without any intermediate purification steps (*12*). CYP6B1 was expressed in *Sf9* insect cells, and the membrane fraction was solubilized using a high concentration of cholate (500 mM). MSP1 was added to the solubilized membrane fraction in an approximate MSP:lipid:detergent molar ratio of 1:100:200. Removal of cholate by Bio-Beads caused Nanodiscs to self-assemble while incorporating all of the membrane proteins expressed by the *Sf9* insect cells, including the overexpressed CYP6B1. MSP1 bears a hexahistidine metal affinity tag, allowing the target to be purified by Ni affinity chromatography. CYP6B1-containing Nanodiscs were then isolated by collecting fractions from a size-exclusion column that displayed a heme absorbance signal at 417 nm. SDS−PAGE of the resulting sample showed that the isolated CYP6B1 was relatively pure, and its structural integrity was verified by a CO-bound difference spectrum and a substrate-induced type I shift of the heme absorbance signal. This demonstrates that Nanodiscs can be used to isolate heterologously expressed membrane proteins and maintain them in a lipid bilayer throughout the purification process. This minimizes the exposure of membrane proteins to detergent, and any consequent structural disruption or functional interference.

In subsequent work, the plant enzyme CYP73A5 was coexpressed with a housefly CPR in *Sf9* insect cells and isolated using Nanodiscs (*14*). CYP73A5 in Nanodiscs displayed a normal CO difference spectrum and bound its substrate *tert*-cinnamic acid (*t*-CA) with an affinity comparable to that of CYP73A5 in microsomes. This indicates that the incorporated CYP73A5 is structurally intact. Crucially, CYP73A5 alone expressed in insect cells and isolated using Nanodiscs displayed no *t*-CA hydroxylation activity. However, when CPR was coexpressed with CYP73A5 and the membrane fraction was incorporated into Nanodiscs, a certain subpopulation of Nanodiscs coincorporated CYP73A5 and CPR. The fastest-eluting (highest-diameter) SEC fractions that displayed absorbance signals at 417 nm (CYP73A5) and 456 nm (CPR) were collected and concentrated, and their homogeneity and stability were verified by reinjection onto the size-exclusion column. These fractions with co-incorporated CYP73A5, and CPR displayed *t*-CA hydroxylation activity when NADPH was added, suggesting that at least some Nanodiscs contained CYP73A5 and CPR on the same side of the bilayer in a productive orientation.

Nanodiscs have been used in several studies of CYP3A4, a major drug-metabolizing enzyme. CYP3A4 is a promiscuous enzyme with a large, conformationally dynamic active site that can accommodate multiple substrate and effector molecules, often leading to allosteric kinetic behavior (*82*, *83*). Detailed information about binding of ligand to CYP3A4 is important in understanding therapeutically relevant drug−drug interactions. CYP3A4 studies are hampered by the same

problems of conformational heterogeneity (*84*−*88*) as other membrane-bound CYPs. Nanodiscs provide a possible way to solubilize CYP3A4 and maintain it monomerically at the high concentrations needed to investigate cooperativity in ligand binding, and consequent allosteric kinetics in catalysis. Initial studies with CYP3A4 in Nanodiscs (*13*) investigated testosterone binding and turnover by CYP3A4. As monitored by absorbance spectroscopy, testosterone bound to CYP3A4 with apparent positive cooperativity, with at least three possible binding modes in the CYP3A4−Nanodisc complex. CYP3A4 in Nanodiscs retained the ability to metabolize testosterone to 6β-hydroxytestosterone using the so-called "peroxide shunt". (In this modification of the CYP catalytic pathway, the two single-electron reductions of CYP normally carried out by CPR or cytochrome b_5 are instead effected by an added source of peroxide, such as hydrogen peroxide or cumene peroxide.) This study showed that Nanodiscs were suitable model membranes for studying the ligand binding and catalytic behavior of CYP3A4. SAXS studies of the CYP3A4−Nanodisc complex indicated that, as expected, only a small part of the CYP3A4 molecule is embedded in the Nanodisc bilayer.

A subsequent study (*15*) investigated the effect of CYP3A4 oligomeric heterogeneity on the kinetics of enzyme reduction by dithionite. Stopped-flow absorbance spectroscopy was used to measure the rates of dithionite reduction of CYP3A4 in solution, CYP3A4 monomerized by the detergent Emulgen 913, CYP3A4 in Nanodiscs, and CYP3A4 in lipid-rich and lipid-poor proteoliposomes. CYP3A4 in solution and in lipid-poor proteoliposomes exhibited additional kinetic phases in its reduction by diothionite that were not observed for the enzyme in Emulgen 913, Nanodiscs, or lipid-rich proteoliposomes. This suggests that CYP3A4 structure and/or dynamics in the former two systems are affected by conformational heterogeneity that is absent in the latter three systems.

CYP3A4 in Nanodiscs was also used to study the effect of ligands on CYP autoxidation kinetics (*16*). This is a crucial step in the CYP catalytic pathway, where the ferrous−oxy complex is converted to a ferric−superoxy form. Autoxidation kinetics were measured by reducing CYP3A4 incorporated in Nanodiscs and using stopped-flow absorbance spectroscopy to monitor its mixing with oxygenated aqueous buffer. An initial fast phase represented formation of the ferrous−oxy complex, and a slower phase represented conversion to the ferric−superoxy complex. Earlier experiments performed without Nanodiscs resulted in multiphasic autoxidation kinetics, but it was unclear whether this was an artifact due to CYP3A4 conformational heterogeneity or an accurate reflection of in vivo behavior (*89*). In this work, incorporation into Nanodiscs ensured that CYP3A4 was monomeric, which in turn resulted in monophasic kinetics for this conversion. CYP3A4 in Nanodiscs thus provide an excellent system for studying the effect of various ligands on autoxidation kinetics and consequent effects on CYP catalytic efficiency.

Depending on the relative affinities of a ligand for the bilayer and for the CYP3A4 active site, the presence of the lipid phase can increase or decrease the apparent binding affinity of a ligand for CYP3A4 (*90*). To deconvolute these possibly conflicting effects, it is necessary to accurately measure the affinity of small molecules for Nanodiscs themselves. Nanodiscs are particularly attractive model membranes for studying small-molecule binding because of the stable, well-defined nature of their bilayer. A variety of analytical techniques can be employed, including environment-sensitive ligand fluorescence or absorbance, ligand-induced changes in the intrinsic fluorescence of MSP tryptophan residues, isothermal calorimetry, and surface plasmon resonance. Nanodiscs also allow for the detailed study of nonideal (cooperative) binding by small molecules, where a ligand's affinity for the membrane is affected by the prior concentration of bound ligand.

The routes of substrate access to and product egress from the CYP3A4 active site are currently unknown. Kinetic experiments using stopped-flow spectroscopy and surface plasmon resonance are underway to determine whether ligands transiently occupy the Nanodisc bilayer before binding to the CYP3A4 active site (indicating they must enter the active site via the membrane phase) or whether they bind directly from solution.

Other significant integral membrane proteins that have been studied using Nanodiscs include bacterial chemoreceptors (*22*). These proteins modulate chemotaxis in bacteria such as *E. coli* by sensing the chemical environment around the cell and transducing the signal to the flagellar rotary motor. The *E. coli* aspartate chemoreceptor Tar was incorporated into Nanodiscs prepared with MSP1D1E3 (a deletion of 11 N-terminal residues combined with an insertion of three internal 22-mer helices) and detergent-stabilized *E. coli* membrane lipids. The minimal structural unit of Tar was found to be a homodimer. In terms of function, Tar homodimers were capable of transmembrane signaling (as monitored by Tar methylation and deamidation in response to ligand binding) but could not activate the downstream kinases necessary for signal transduction to the flagellar rotary motor. It was found that the minimal functional unit of Tar capable of downstream signaling was a trimer of homodimers. While this quarternary structure is supported by crystallography (*91*) and cross-linking studies (*92*), its functional significance could not have been obtained without incorporation into the well-defined, isolated lipid bilayer provided by Nanodiscs.

These examples demonstrate that phospholipid bilayer Nanodiscs are powerful and versatile model membranes that can simplify investigations of the structure and function of a wide variety of biologically relevant membrane proteins, including cytochrome P450s and GPCRs. Nanodiscs may provide a general solution for membrane proteins that could help extend our knowledge about them to a level commensurate with their biological and pharmacological significance. Nanodiscs are also good systems for the study of biological membranes, in terms of small-molecule binding and phase transition behavior, using a wide variety of techniques. Their utility ultimately stems from their stable, monodisperse, well-defined structure.

ACKNOWLEDGMENT

We gratefully acknowledge Dr. Ilia Denisov and Dr. Tim Bayburt for helpful discussions.

REFERENCES

1. Wallin, E., and von Heijne, G. (1998) Genome-wide analysis of integral membrane proteins from eubacterial, archaean, and eukaryotic organisms, *Protein Sci. 7*, 1029−1038.

2. Drews, J. (2000) Drug discovery: A historical perspective, *Science 287*, 1960−1964.
3. Wishart, D. S., Knox, C., Guo, A. C., Shrivastava, S., Hassanali, M., Stothard, P., Chang, Z., and Woolsey, J. (2006) DrugBank: A comprehensive resource for in silico drug discovery and exploration, *Nucleic Acids Res. 34*, D668−D672.
4. Lundstrom, K. H. (2006) *Structural Genomics of Membrane Proteins*, CRC Press, Boca Raton, FL.
5. Seddon, A. M., Curnow, P., and Booth, P. J. (2004) Membrane proteins, lipids and detergents: Not just a soap opera, *Biochim. Biophys. Acta 1666*, 105−117.
6. Bayburt, T. H., Grinkova, Y. V., and Sligar, S. G. (2002) Self-assembly of discoidal phospholipid bilayer nanoparticles with membrane scaffold proteins, *Nano Lett. 2*, 853−856.
7. Denisov, I. G., Grinkova, Y. V., Lazarides, A. A., and Sligar, S. G. (2004) Directed self-assembly of monodisperse phospholipid bilayer Nanodiscs with controlled size, *J. Am. Chem. Soc. 126*, 3477−3487.
8. Sligar, S. G. (2003) Finding a single-molecule solution for membrane proteins, *Biochem. Biophys. Res. Commun. 312*, 115−119.
9. Shaw, A. W., McLean, M. A., and Sligar, S. G. (2004) Phospholipid phase transitions in homogeneous nanometer scale bilayer discs, *FEBS Lett. 556*, 260−264.
10. Denisov, I. G., McLean, M. A., Shaw, A. W., Grinkova, Y. V., and Sligar, S. G. (2005) Thermotropic phase transition in soluble nanoscale lipid bilayers, *J. Phys. Chem. B 109*, 15580−15588.
11. Bayburt, T. H., and Sligar, S. G. (2002) Single-molecule height measurements on microsomal cytochrome P450 in nanometer-scale phospholipid bilayer disks, *Proc. Natl. Acad. Sci. U.S.A. 99*, 6725−6730.
12. Civjan, N. R., Bayburt, T. H., Schuler, M. A., and Sligar, S. G. (2003) Direct solubilization of heterologously expressed membrane proteins by incorporation into nanoscale lipid bilayers, *BioTechniques 35*, 556−560, 562−563.
13. Baas, B. J., Denisov, I. G., and Sligar, S. G. (2004) Homotropic cooperativity of monomeric cytochrome P450 3A4 in a nanoscale native bilayer environment, *Arch. Biochem. Biophys. 430*, 218−228.
14. Duan, H., Civjan, N. R., Sligar, S. G., and Schuler, M. A. (2004) Co-incorporation of heterologously expressed *Arabidopsis* cytochrome P450 and P450 reductase into soluble nanoscale lipid bilayers, *Arch. Biochem. Biophys. 424*, 141−153.
15. Davydov, D. R., Fernando, H., Baas, B. J., Sligar, S. G., and Halpert, J. R. (2005) Kinetics of dithionite-dependent reduction of cytochrome P450 3A4: Heterogeneity of the enzyme caused by its oligomerization, *Biochemistry 44*, 13902−13913.
16. Denisov, I. G., Grinkova, Y. V., Baas, B. J., and Sligar, S. G. (2006) The Ferrous-Dioxygen Intermediate in Human Cytochrome P450 3A4: Substrate Dependence of Formation and Decay Kinetics, *J. Biol. Chem. 281*, 23313−23318.
17. Bayburt, T. H., Carlson, J. W., and Sligar, S. G. (1998) Reconstitution and imaging of a membrane protein in a nanometer-size phospholipid bilayer, *J. Struct. Biol. 123*, 37−44.
18. Bayburt, T. H., Carlson, J. W., and Sligar, S. G. (2000) Single molecule height measurements on a membrane protein in nanometer-scale phospholipid bilayer disks, *Langmuir 16*, 5993−5997.
19. Bayburt, T. H., and Sligar, S. G. (2003) Self-assembly of single integral membrane proteins into soluble nanoscale phospholipid bilayers, *Protein Sci. 12*, 2476−2481.
20. Bayburt, T. H., Grinkova, Y. V., and Sligar, S. G. (2006) Assembly of single bacteriorhodopsin trimers in bilayer nanodiscs, *Arch. Biochem. Biophys. 450*, 215−222.
21. Leitz, A. J., Bayburt, T. H., Barnakov, A. N., Springer, B. A., and Sligar, S. G. (2006) Functional reconstitution of β2-adrenergic receptors utilizing self-assembling Nanodisc technology, *BioTechniques 40*, 601−602, 604, 606, passim.
22. Boldog, T., Grimme, S., Li, M., Sligar, S. G., and Hazelbauer, G. L. (2006) Nanodiscs separate chemoreceptor oligomeric states and reveal their signaling properties, *Proc. Natl. Acad. Sci. U.S.A. 103*, 11509−11514.
23. Beschiaschvili, G., and Seelig, J. (1992) Peptide binding to lipid bilayers. Nonclassical hydrophobic effect and membrane-induced pK shifts, *Biochemistry 31*, 10044−10053.
24. Atkinson, D., and Small, D. M. (1986) Recombinant lipoproteins: Implications for structure and assembly of native lipoproteins, *Annu. Rev. Biophys. Biophys. Chem. 15*, 403−456.
25. Ohashi, R., Mu, H., Wang, X., Yao, Q., and Chen, C. (2005) Reverse cholesterol transport and cholesterol efflux in atherosclerosis, *Q. J. Med. 98*, 845−856.
26. Brouillette, C. G., Anantharamaiah, G. M., Engler, J. A., and Borhani, D. W. (2001) Structural models of human apolipoprotein A-I: A critical analysis and review, *Biochim. Biophys. Acta 1531*, 4−46.
27. Gianazza, E., Eberini, I., Sirtori, C. R., Franceschini, G., and Calabresi, L. (2002) Size is a major determinant of dissociation and denaturation behaviour of reconstituted high-density lipoproteins, *Biochem. J. 366*, 245−253.
28. Tricerri, M. A., Sanchez, S. A., Arnulphi, C., Durbin, D. M., Gratton, E., and Jonas, A. (2002) Interaction of apolipoprotein A-I in three different conformations with palmitoyl oleoyl phosphatidylcholine vesicles, *J. Lipid Res. 43*, 187−197.
29. Maiorano, J. N., Jandacek, R. J., Horace, E. M., and Davidson, W. S. (2004) Identification and structural ramifications of a hinge domain in apolipoprotein A-I discoidal high-density lipoproteins of different size, *Biochemistry 43*, 11717−11726.
30. Cheung, M. C., Segrest, J. P., Albers, J. J., Cone, J. T., Brouillette, C. G., Chung, B. H., Kashyap, M., Glasscock, M. A., and Anantharamaiah, G. M. (1987) Characterization of high density lipoprotein subspecies: Structural studies by single vertical spin ultracentrifugation and immunoaffinity chromatography, *J. Lipid Res. 28*, 913−929.
31. Klon, A. E., Jones, M. K., Segrest, J. P., and Harvey, S. C. (2000) Molecular belt models for the apolipoprotein A-I Paris and Milano mutations, *Biophys. J. 79*, 1679−1685.
32. Saito, H., Dhanasekaran, P., Nguyen, D., Deridder, E., Holvoet, P., Lund-Katz, S., and Phillips, M. C. (2004) α-Helix formation is required for high affinity binding of human apolipoprotein A-I to lipids, *J. Biol. Chem. 279*, 20974−20981.
33. Rogers, D. P., Roberts, L. M., Lebowitz, J., Datta, G., Anantharamaiah, G. M., Engler, J. A., and Brouillette, C. G. (1998) The lipid-free structure of apolipoprotein A-I: Effects of amino-terminal deletions, *Biochemistry 37*, 11714−11725.
34. Rogers, D. P., Brouillette, C. G., Engler, J. A., Tendian, S. W., Roberts, L., Mishra, V. K., Anantharamaiah, G. M., Lund-Katz, S., Phillips, M. C., and Ray, M. J. (1997) Truncation of the amino terminus of human apolipoprotein A-I substantially alters only the lipid-free conformation, *Biochemistry 36*, 288−300.
35. Ajees, A. A., Anantharamaiah, G. M., Mishra, V. K., Hussain, M. M., and Murthy, H. M. (2006) Crystal structure of human apolipoprotein A-I: Insights into its protective effect against cardiovascular diseases, *Proc. Natl. Acad. Sci. U.S.A. 103*, 2126−2131.
36. Borhani, D. W., Rogers, D. P., Engler, J. A., and Brouillette, C. G. (1997) Crystal structure of truncated human apolipoprotein A-I suggests a lipid-bound conformation, *Proc. Natl. Acad. Sci. U.S.A. 94*, 12291−12296.
37. Rogers, D. P., Roberts, L. M., Lebowitz, J., Engler, J. A., and Brouillette, C. G. (1998) Structural analysis of apolipoprotein A-I: Effects of amino- and carboxy-terminal deletions on the lipid-free structure, *Biochemistry 37*, 945−955.
38. Roberts, L. M., Ray, M. J., Shih, T. W., Hayden, E., Reader, M. M., and Brouillette, C. G. (1997) Structural analysis of apolipoprotein A-I: Limited proteolysis of methionine-reduced and -oxidized lipid-free and lipid-bound human apo A-I, *Biochemistry 36*, 7615−7624.
39. Atkinson, D., Smith, H. M., Dickson, J., and Austin, J. P. (1976) Interaction of apoprotein from porcine high-density lipoprotein with dimyristoyl lecithin. 1. The structure of the complexes, *Eur. J. Biochem. 64*, 541−547.
40. Andrews, A. L., Atkinson, D., Barratt, M. D., Finer, E. G., Hauser, H., Henry, R., Leslie, R. B., Owens, N. L., Phillips, M. C., and Robertson, R. N. (1976) Interaction of apoprotein from porcine high-density lipoprotein with dimyristoyl lecithin. 2. Nature of lipid-protein interaction, *Eur. J. Biochem. 64*, 549−563.
41. Segrest, J. P. (1977) Amphipathic helixes and plasma lipoproteins: Thermodynamic and geometric considerations, *Chem. Phys. Lipids 18*, 7−22.
42. Wlodawer, A., Segrest, J. P., Chung, B. H., Chiovetti, R., Jr., and Weinstein, J. N. (1979) High-density lipoprotein recombinants: Evidence for a bicycle tire micelle structure obtained by neutron scattering and electron microscopy, *FEBS Lett. 104*, 231−235.
43. Brouillette, C. G., Jones, J. L., Ng, T. C., Kercret, H., Chung, B. H., and Segrest, J. P. (1984) Structural studies of apolipoprotein A-I/phosphatidylcholine recombinants by high-field proton NMR,

nondenaturing gradient gel electrophoresis, and electron microscopy, *Biochemistry 23*, 359−367.
44. Nolte, R. T., and Atkinson, D. (1992) Conformational analysis of apolipoprotein A-I and E-3 based on primary sequence and circular dichroism, *Biophys. J. 63*, 1221−1239.
45. Phillips, J. C., Wriggers, W., Li, Z., Jonas, A., and Schulten, K. (1997) Predicting the structure of apolipoprotein A-I in reconstituted high-density lipoprotein disks, *Biophys. J. 73*, 2337−2346.
46. Koppaka, V., Silvestro, L., Engler, J. A., Brouillette, C. G., and Axelsen, P. H. (1999) The structure of human lipoprotein A-I. Evidence for the "belt" model, *J. Biol. Chem. 274*, 14541−14544.
47. Segrest, J. P., Jones, M. K., Klon, A. E., Sheldahl, C. J., Hellinger, M., De Loof, H., and Harvey, S. C. (1999) A detailed molecular belt model for apolipoprotein A-I in discoidal high density lipoprotein, *J. Biol. Chem. 274*, 31755−31758.
48. Tricerri, M. A., Behling Agree, A. K., Sanchez, S. A., Bronski, J., and Jonas, A. (2001) Arrangement of apolipoprotein A-I in reconstituted high-density lipoprotein disks: An alternative model based on fluorescence resonance energy transfer experiments, *Biochemistry 40*, 5065−5074.
49. Davidson, W. S., and Hilliard, G. M. (2003) The spatial organization of apolipoprotein A-I on the edge of discoidal high density lipoprotein particles: A mass specrometry study, *J. Biol. Chem. 278*, 27199−27207.
50. Silva, R. A., Hilliard, G. M., Li, L., Segrest, J. P., and Davidson, W. S. (2005) A mass spectrometric determination of the conformation of dimeric apolipoprotein A-I in discoidal high density lipoproteins, *Biochemistry 44*, 8600−8607.
51. Thomas, M. J., Bhat, S., and Sorci-Thomas, M. G. (2006) The use of chemical cross-linking and mass spectrometry to elucidate the tertiary conformation of lipid-bound apolipoprotein A-I, *Curr. Opin. Lipidol. 17*, 214−220.
52. Bhat, S., Sorci-Thomas, M. G., Alexander, E. T., Samuel, M. P., and Thomas, M. J. (2005) Intermolecular contact between globular N-terminal fold and C-terminal domain of ApoA-I stabilizes its lipid-bound conformation: Studies employing chemical cross-linking and mass spectrometry, *J. Biol. Chem. 280*, 33015−33025.
53. Gorshkova, I. N., Liu, T., Kan, H. Y., Chroni, A., Zannis, V. I., and Atkinson, D. (2006) Structure and stability of apolipoprotein a-I in solution and in discoidal high-density lipoprotein probed by double charge ablation and deletion mutation, *Biochemistry 45*, 1242−1254.
54. Martin, D. D., Budamagunta, M. S., Ryan, R. O., Voss, J. C., and Oda, M. N. (2006) Apolipoprotein A-I assumes a "looped belt" conformation on reconstituted high density lipoprotein, *J. Biol. Chem. 281*, 20418−20426.
55. Panagotopulos, S. E., Horace, E. M., Maiorano, J. N., and Davidson, W. S. (2001) Apolipoprotein A-I adopts a belt-like orientation in reconstituted high density lipoproteins, *J. Biol. Chem. 276*, 42965−42970.
56. Li, H., Lyles, D. S., Thomas, M. J., Pan, W., and Sorci-Thomas, M. G. (2000) Structural determination of lipid-bound ApoA-I using fluorescence resonance energy transfer, *J. Biol. Chem. 275*, 37048−37054.
57. Li, Y., Kijac, A. Z., Sligar, S. G., and Rienstra, C. M. (2006) Structural analysis of nanoscale self-assembled discoidal lipid bilayers by solid-state NMR spectroscopy, *Biophys. J. 91*, 3819−3828.
58. Segrest, J. P., Harvey, S. C., and Zannis, V. (2000) Detailed molecular model of apolipoprotein A-I on the surface of high-density lipoproteins and its functional implications, *Trends Cardiovasc. Med. 10*, 246−252.
59. Heller, H., Schaefer, M., and Schulten, K. (1993) Molecular Dynamics Simulation of a Bilayer of 200 Lipids in the Gel and in the Liquid-Crystal Phases, *J. Phys. Chem. 97*, 8343−8360.
60. Klon, A. E., Segrest, J. P., and Harvey, S. C. (2002) Molecular dynamics simulations on discoidal HDL particles suggest a mechanism for rotation in the apo A-I belt model, *J. Mol. Biol. 324*, 703−721.
61. Shih, A. Y., Denisov, I. G., Phillips, J. C., Sligar, S. G., and Schulten, K. (2005) Molecular dynamics simulations of discoidal bilayers assembled from truncated human lipoproteins, *Biophys. J. 88*, 548−556.
62. Shih, A. Y., Arkhipov, A., Freddolino, P. L., and Schulten, K. (2006) Coarse grained protein-lipid model with application to lipoprotein particles, *J. Phys. Chem. B 110*, 3674−3684.
63. Catte, A., Patterson, J. C., Jones, M. K., Jerome, W. G., Bashtovyy, D., Su, Z., Gu, F., Chen, J., Aliste, M. P., Harvey, S. C., Li, L., Weinstein, G., and Segrest, J. P. (2006) Novel changes in discoidal high density lipoprotein morphology: A molecular dynamics study, *Biophys. J. 90*, 4345−4360.
64. Feller, S. E., Venable, R. M., and Pastor, R. W. (1997) Computer simulation of a DPPC phospholipid bilayer: Structural changes as a function of molecular surface area, *Langmuir 13*, 6555−6561.
65. Marrink, S. J., de Vries, A. H., and Mark, A. E. (2004) Coarse grained model for semiquantitative lipid simulations, *J. Phys. Chem. B 108*, 750−760.
66. Janoff, A. S., Ed. (1999) *Liposomes: Rational Design*, Marcel Dekker, New York.
67. Bangham, A. D., Standish, M. M., and Watkins, J. C. (1965) Diffusion of univalent ions across the lamellae of swollen phospholipids, *J. Mol. Biol. 13*, 238−252.
68. Bangham, A. D. (1972) Lipid bilayers and biomembranes, *Annu. Rev. Biochem. 41*, 753−776.
69. Woodle, M. C., and Papahadjopoulos, D. (1989) Liposome preparation and size characterization, *Methods Enzymol. 171*, 193−217.
70. Otake, K., Imura, T., Sakai, H., and Abe, M. (2001) Development of a new preparation method of liposomes using supercritical carbon dioxide, *Langmuir 17*, 3898−3901.
71. Otake, K., Shimomura, T., Goto, T., Imura, T., Furuya, T., Yoda, S., Takebayashi, Y., Sakai, H., and Abe, M. (2006) Preparation of liposomes using an improved supercritical reverse phase evaporation method, *Langmuir 22*, 2543−2550.
72. Shah, D. O., Ed. (1998) *Micelles, Microemulsions, and Monolayers*, Marcel Dekker, New York.
73. Ollivon, M., Lesieur, S., Grabielle-Madelmont, C., and Paternostre, M. (2000) Vesicle reconstitution from lipid-detergent mixed micelles, *Biochim. Biophys. Acta 1508*, 34−50.
74. Almgren, M. (2000) Mixed micelles and other structures in the solubilization of bilayer lipid membranes by surfactants, *Biochim. Biophys. Acta 1508*, 146−163.
75. Edwards, K., Johnsson, M., Karlsson, G., and Silvander, M. (1997) Effect of polyethyleneglycol-phospholipids on aggregate structure in preparations of small unilamellar liposomes, *Biophys. J. 73*, 258−266.
76. Johnsson, M., and Edwards, K. (2001) Phase behavior and aggregate structure in mixtures of dioleoylphosphatidylethanolamine and poly(ethylene glycol)-lipids, *Biophys. J. 80*, 313−323.
77. Johnsson, M., and Edwards, K. (2003) Liposomes, disks, and spherical micelles: Aggregate structure in mixtures of gel phase phosphatidylcholines and poly(ethylene glycol)-phospholipids, *Biophys. J. 85*, 3839−3847.
78. Johansson, E., Engvall, C., Arfvidsson, M., Lundahl, P., and Edwards, K. (2005) Development and initial evaluation of PEG-stabilized bilayer disks as novel model membranes, *Biophys. Chem. 113*, 183−192.
79. Heyn, M. P., Blume, A., Rehorek, M., and Dencher, N. A. (1981) Calorimetric and fluorescence depolarization studies on the lipid phase transition of bacteriorhodopsin−dimyristoylphosphatidylcholine vesicles, *Biochemistry 20*, 7109−7115.
80. Scott, E. E., White, M. A., He, Y. A., Johnson, E. F., Stout, C. D., and Halpert, J. R. (2004) Structure of mammalian cytochrome P450 2B4 complexed with 4-(4-chlorophenyl)imidazole at 1.9-Å resolution: Insight into the range of P450 conformations and the coordination of redox partner binding, *J. Biol. Chem. 279*, 27294−27301.
81. Wang, M., Roberts, D. L., Paschke, R., Shea, T. M., Masters, B. S., and Kim, J. J. (1997) Three-dimensional structure of NADPH-cytochrome P450 reductase: Prototype for FMN- and FAD-containing enzymes, *Proc. Natl. Acad. Sci. U.S.A. 94*, 8411−8416.
82. Yoon, M. Y., Campbell, A. P., and Atkins, W. M. (2004) "Allosterism" in the elementary steps of the cytochrome P450 reaction cycle, *Drug Metab. Rev. 36*, 219−230.
83. Atkins, W. M. (2005) Non-Michaelis-Menten kinetics in cytochrome P450-catalyzed reactions, *Annu. Rev. Pharmacol. Toxicol. 45*, 291−310.
84. Koley, A. P., Robinson, R. C., and Friedman, F. K. (1996) Cytochrome P450 conformation and substrate interactions as probed by CO binding kinetics, *Biochimie 78*, 706−713.
85. Koley, A. P., Buters, J. T., Robinson, R. C., Markowitz, A., and Friedman, F. K. (1997) Differential mechanisms of cytochrome P450 inhibition and activation by α-naphthoflavone, *J. Biol. Chem. 272*, 3149−3152.
86. Koley, A. P., Robinson, R. C., Markowitz, A., and Friedman, F. K. (1997) Drug-drug interactions: Effect of quinidine on nifedipine binding to human cytochrome P450 3A4, *Biochem. Pharmacol. 53*, 455−460.

87. Davydov, D. R., Halpert, J. R., Renaud, J. P., and Hui Bon Hoa, G. (2003) Conformational heterogeneity of cytochrome P450 3A4 revealed by high pressure spectroscopy, *Biochem. Biophys. Res. Commun. 312*, 121−130.

88. Kumar, S., Davydov, D. R., and Halpert, J. R. (2005) Role of cytochrome B5 in modulating peroxide-supported cyp3a4 activity: Evidence for a conformational transition and cytochrome P450 heterogeneity, *Drug Metab. Dispos. 33*, 1131−1136.

89. Oprian, D. D., Gorsky, L. D., and Coon, M. J. (1983) Properties of the oxygenated form of liver microsomal cytochrome P-450, *J. Biol. Chem. 258*, 8684−8691.

90. Nath, A., Baas, B. J., Sligar, S. G., and Atkins, W. M. (2006) Ligand Binding to Cytochrome P450 3A4 in Phospholipid Bilayer Nanodiscs: The Effect of Model Membranes, manuscript in preparation.

91. Kim, K. K., Yokota, H., and Kim, S. H. (1999) Four-helical-bundle structure of the cytoplasmic domain of a serine chemotaxis receptor, *Nature 400*, 787−792.

92. Studdert, C. A., and Parkinson, J. S. (2004) Crosslinking snapshots of bacterial chemoreceptor squads, *Proc. Natl. Acad. Sci. U.S.A. 101*, 2117−2122.

93. Li, Y., Kijac, A. Z., Sligar, S. G., and Rienstra, C. M. (2006) Structural Analysis of Nanoscale Self-Assembled Discoidal Lipid Bilayers by Solid-State NMR Spectroscopy, *Biophys. J.* (in press).

94. DeLano, W. L. (2002) *The PyMOL Molecular Graphics System*, DeLano Scientific, San Carlos, CA.

95. Yano, J. K., Wester, M. R., Schoch, G. A., Griffin, K. J., Stout, C. D., and Johnson, E. F. (2004) The structure of human microsomal cytochrome P450 3A4 determined by X-ray crystallography to 2.05-Å resolution, *J. Biol. Chem. 279*, 38091−38094.

96. Palczewski, K., Kumasaka, T., Hori, T., Behnke, C. A., Motoshima, H., Fox, B. A., Le Trong, I., Teller, D. C., Okada, T., Stenkamp, R. E., Yamamoto, M., and Miyano, M. (2000) Crystal structure of rhodopsin: A G protein-coupled receptor, *Science 289*, 739−745.

97. Yeh, J. I., Biemann, H. P., Prive, G. G., Pandit, J., Koshland, D. E., Jr., and Kim, S. H. (1996) High-resolution structures of the ligand binding domain of the wild-type bacterial aspartate receptor, *J. Mol. Biol. 262*, 186−201.

BI602371N